

Original paper

Gold-bearing quartz veins of the Bělčice ore district, Bohemian Massif: evidence for incursion of metamorphic fluids into a granodiorite body and for isothermal mixing between two types of metamorphic fluids

Jiří ZACHARIÁŠ*, Tomáš NOVÁK

Institute of Geochemistry, Mineralogy and Mineral Resources, Charles University, Albertov 6, 128 43 Prague 2, Czech Republic; zachar@natur.cuni.cz

* *Corresponding author*



Gold-bearing quartz veins of the Bělčice ore district are hosted by I-type Variscan Blatná granodiorite of the Central Bohemian Plutonic Complex. The quartz gangue precipitated from aqueous-carbonic fluids (3–7 wt. % NaCl eq.) with significant methane admixture (up to 15 mol. % of CH₄) at c. 350–400 °C and 200–400 MPa. The ore stage including gold precipitation occurred at lower temperatures (300 to 250 °C) and pressures (~ 100 MPa) from aqueous fluids. The isotope composition of the quartz and carbonate gangue indicates progressively heavier oxygen of the parental fluid ($\delta^{18}\text{O}_{\text{fluid}}$ from ~ 9–10 ‰ to 10–14 ‰ SMOW). This suggests ingress of metamorphic fluids equilibrated with metasedimentary country rocks into an environment dominated by I-type granitoids. Invasion of external metamorphic fluids is also supported by nearly isothermal mixing trends in aqueous fluids as documented by salinity variations (from 5.5 to 0 wt. % NaCl eq.).

Keywords: orogenic gold, fluid inclusions, stable isotopes, chlorite thermometry, Moldanubian Zone, Bohemian Massif

Received: January 15, 2009; accepted: March 12, 2009; handling editor: S. Vrána

1. Introduction

Orogenic gold deposits are typically formed from metamorphic fluids released during the intracrustal processes connected with collision and crustal thickening (e.g. Groves et al. 1998, 2003; Goldfarb et al. 2001). For some deposits, however, a magmatic component in the fluid was documented or at least suggested (e.g. Burrows and Spooner 1987; Thompson et al. 1999). In areas where magmatic and metamorphic events overlapped in time, distinction between magmatic and metamorphic fluids is, however, often ambiguous. A significant magmatic contribution is also suggested for intrusion-related gold deposits (e.g. Lang and Baker 2001; Baker 2002), a relatively new class of gold deposits, which seem to also include the Mokrsko (Morávek et al. 1989; Boiron et al. 2001) and Petrůvka hora (Zachariáš et al. 2001) gold deposits in the Bohemian Massif (Fig. 1a).

In the central part of the Bohemian Massif numerous gold deposits are located along the northwestern boundary of the Variscan Central Bohemian Plutonic Complex (CBPC; Fig. 1a). With respect to mineralogy, hydrothermal alterations, fluid inclusion and stable isotope data these deposits could be classified as mesothermal (orogenic) gold deposits (Zachariáš et al. 1997). Relevant

is that formation of individual gold deposits followed shortly after intrusive activity of the CBPC. The ages of early to main mineralization stages of the individual gold deposits span from ~349 to ~338 Ma (Re-Os on molybdenite; Zachariáš and Stein 2001) and thus overlap significantly major intrusion activity of the CBPC (~354 to ~336 Ma; e.g. Holub et al. 1997; Dörr et al. 1998; Janoušek and Gerdes 2003).

In order to evaluate metamorphic, magmatic or meteoric water contributions, we performed fluid inclusion and stable isotope studies of the quartz-carbonate gangue from various localities within the Bělčice ore district. Veins in this district are hosted exclusively by granitoids of the CBPC.

2. Geology and mining history

The Bělčice ore district is located c. 80 km south of Prague, between the towns of Bělčice and Lnáře. The district can be separated into the northern (Újezdec u Bělčic, Kněžská hora and adit Barbora), central (Borek and Hory) and southern (Na Skřipici) parts (Fig. 1b). The Bělčice ore district and the adjacent Kasejovice ore district to the west were treated by some authors as a single Kasejovice–Bělčice ore district.

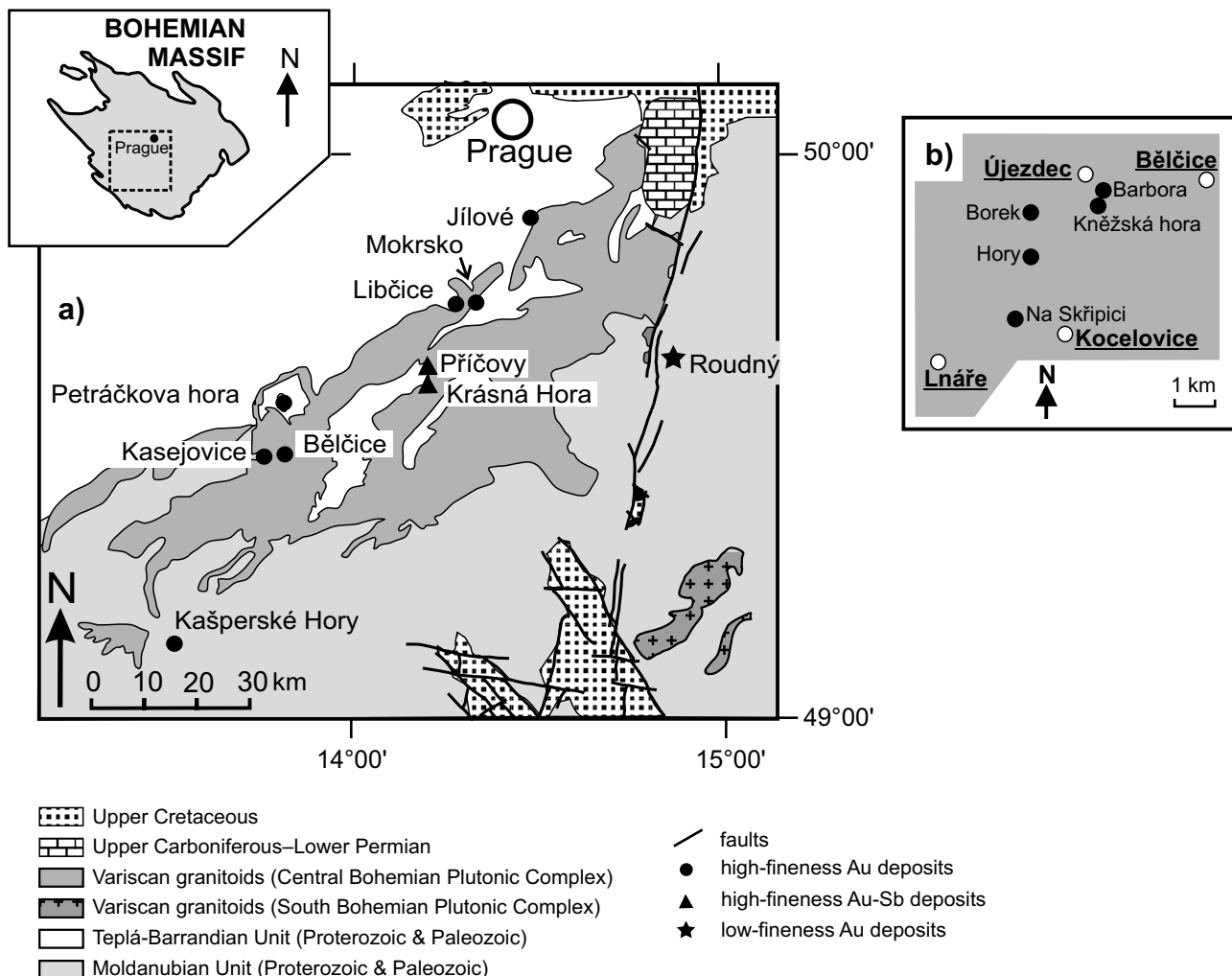


Fig. 1a – Geological context and position of gold deposits associated with the Central Bohemian Plutonic Complex. The small inset shows the location of the main figure within the Bohemian Massif. **b** – Localization of mining works within the Bělčice ore district.

2.1. History

Although gold exploration in the Bělčice district can be traced back to the 14th century, the most intense mining and exploration commenced at the beginning of the 20th century. The heart of the mining activity was in the Kněžská hora area. Four exploration shafts 3 to 18.6 m deep were dug here before 1907, followed by the 340 m long Barbora exploration adit (1907–1917) and a 136.8 m deep Josef mining shaft. About 45 quartz veins were identified and some of them were explored. The largest vein (vein No. 39) was selectively mined (average vein thickness 0.23 m, mined vein area 268 m²) and yielded about 154 t of quartz gangue with an average gold content of 13.3 g/t Au and 2.054 kg of total gold production. Despite the relatively high gold contents at all localities, the district and individual deposits were finally designated as uneconomic. The ore potential was later re-evaluated dur-

ing the World War II (1942–1944; Koutek 1946) and in 1982–1988 (Vlašimský and Píša 1985; Váňa et al. 1988), always with negative conclusions.

2.2. Geology

Gold-bearing quartz veins of the Bělčice ore district are hosted by amphibole-biotite granodiorite of the Blatná suite of the CBPC. Minor aplite-pegmatite dykes or lenses, and a granodiorite porphyry dyke and xenoliths were also found. No significant differences in the vein morphology, ore mineralogy or in the elemental signature of mineralization were found between individual mines and district parts.

The quartz veins are 0.01–1 m thick (typically 0.1–0.3 m) and the length along the strike varies from several meters to about 70 m. The main vein (No. 39) occupies

a large tectonic zone trending NW–SW and dipping 45–60° to the SE. The length of this vein along the dip was 140 m, while that along the strike was only 35 m. This relationship, with the vertical extent of quartz vein exceeding the horizontal one several times, was also confirmed for other veins. The gold content varied from 2.5 to 23.1 g/t in individual samples.

2.3. Mineralogy

The mineralogy of the Bělčice ore district was studied by Hofmann and Slavík (1913), Sobotka (1966) and Litochleb (1984). The mineral association is simple; veins are dominated by massive milky quartz with low sulfide content, but with locally abundant scheelite and molybdenite. Aggregates of pyrrhotite, arsenopyrite, molybdenite or pyrite are up to 2 cm across. Gold is typically 10–40 µm in size and contains 3 to 11.8 wt. % Ag and up to 1.1 % Hg (Malec and Novák 1982).

Litochleb (1984) distinguished three mineralization stages, based on samples from the Barbora adit:

- 1st stage: quartz-1, K-feldspar, scheelite-1;
- 2nd stage: quartz-2, scheelite-2, arsenopyrite, pyrrhotite, pyrite-1, chalcopyrite, molybdenite, native bismuth, bismuthinite, joseite, tetradymite, native gold;
- 3rd stage: pyrite-2, calcite, chlorite, sericite.

Among the sulfides, pyrrhotite, arsenopyrite and molybdenite are the most frequent. Arsenopyrite forms crystals up to several mm in size, frequently occurring in clusters along vein margins or along fractures in the quartz gangue. Molybdenite forms grains up to 5 mm across or is interspersed with a fine-grained mixture of sulfides and tellurides. Rare chalcopyrite is frequently intergrown with pyrrhotite. Scheelite forms up to 20 × 50 mm large coarse-grained aggregates along the vein margins or more frequently it is disseminated in the quartz gangue. Native bismuth and tellurium minerals occur only as microscopic aggregates. The following succession of ore minerals was established (Litochleb 1984): native bismuth (oldest) → bismuthinite → joseite → tetradymite (youngest). Fluid inclusion and stable isotope study of the Bělčice ore district has not been performed yet. In contrast some limited fluid inclusion data are available for the neighboring Kasejovice district (Zachariáš and Pudilová 2002), mineral association of which however differs in some details (wolframite is present instead of scheelite, molybdenite is rare, sulfides, tellurides and complex sulfides are much more frequent than at the Bělčice district).

3. Methods

The present paper is based on detailed mineralogical and fluid inclusion studies of gangue and ore samples found

at abandoned dumps. In total, 28 samples were collected. Fluid inclusion studies were performed only on 11 of them, representative of all the mineral stages. Fluid inclusion petrographic observations were carried out using a Leica DMPL microscope (magnification up to 1000×), fluid inclusion microthermometry using a Linkam THMSG 600 heating-freezing stage mounted on an Olympus BX-50 microscope with 20× and 50× ULWD objectives. The stage was calibrated using synthetic and natural standards at –56.6 °C (CO₂), 0 °C (H₂O), +31 °C (CO₂), +307 °C (NaNO₃) and +398 °C (K₂Cr₂O₇). The precision of the measurements is ± 0.1 °C from –0 °C to +50 °C and ± 3 °C above 300 °C. Microthermometric data were collected for homogeneous fluid inclusion populations only, such as individual growth zones, three-dimensional clusters or well-defined fluid inclusion trails. The measured phase transitions included the temperature of the first melting (TFM), the melting temperature of the last ice crystal (T_{m-ice}), the melting temperature of solid CO₂ (T_{m-CO₂}), the temperature of CO₂-clathrate dissociation (T_{d-Cl}), the temperature of CO₂-homogenization (T_{h-CO₂}) and the total homogenization temperature (T_{h-tot}). Homogenization occurred either to the liquid (to L) or to the vapor (to V) or via a critical mode (to C). The degree of fill (F) is estimated as the L/(V + L) ratio at 30 °C. Salinities were calculated as wt. % equiv. NaCl using the equations of Bodnar (1993) for aqueous fluids and Bakker (1997, 1999) for aqueous-carbonic fluids. The salinity of aqueous-carbonic fluids includes correction for the admixture of CH₄. The data of Thiery et al. (1994) were used to estimate the composition and molar volume of the gaseous phase in terms of binary CO₂-CH₄ mixture. The isochores were calculated using the equations of Zhang and Frantz (1987) and Bakker (1999) for the H₂O-salt and H₂O-CO₂-CH₄-NaCl systems, respectively.

Oxygen from quartz was liberated for δ¹⁸O measurement using bromine pentafluoride at 500 °C at the Faculty of Science of Charles University (Clayton and Mayeda 1963). Isotope measurements were carried out using a Finnigan MAT 251 mass spectrometer in the laboratory of the Czech Geological Survey, Prague. The total error is ±0.2 ‰. The isotope composition (δ¹⁸O) of fluid was calculated using the quartz-water fractionation equation of Clayton et al. (1972) for 200–500 °C in combination with the trapping temperatures of primary fluid inclusions in quartz gangue or with temperatures inferred from arsenopyrite thermometry.

The oxygen and carbon isotope compositions of calcite were also determined at the Czech Geological Survey. The CO₂ gas was prepared by reaction with 100% phosphoric acid (McCrea 1950). The total error of the isotope measurements is not greater than ± 0.10 ‰. The isotope fluid composition was calculated for so-

lutions in which the aqueous component is dominant ($X_{\text{H}_2\text{O}} \gg X_{\text{H}_2\text{CO}_3/\text{HCO}_3^-}$), with H_2CO_3 as a major species, using the equations of O'Neil et al. (1969) and Ohmoto and Rye (1979) for oxygen and carbon, respectively.

Mineral analyses and back-scattered electron images (BSE) were obtained at the Institute of Geology, Academy of Sciences Czech Republic, Prague, using a Cameca SX-100 electron microprobe. The analytical conditions were: 15 kV accelerating voltage, 4 nA beam current, and 2 μm beam diameter. The standards and spectral lines were: quartz (Si K_{α}), MgO (Mg K_{α}), Al_2O_3 (Al K_{α}), TiO_2 (Ti K_{α}), Fe_2O_3 (Fe K_{α}), diopside (Ca K_{α}), jadeite (Na K_{α}), leucite (K K_{α}), Cr-Mn spinel (Cr K_{α} , Mn K_{α}). Spectrometers used: TAP (Si, Al, Mg, Na), LPET (Ca, K, Ti), and LLIF (Fe, Cr, Mn). The matrix effects were corrected for by the conventional ZAF method.

Analytical setting for arsenopyrite was: 20 kV, 4 nA and 2 μm beam diameter. Elements measured: S (K_{α}), Fe (K_{α}), Co (K_{α}), Ni (K_{α}) and As (L_{α}). Spectrometers used: LTAP (As), PET (S), and LIF (Fe, Co, Ni). Standards used: marcasite (Fe, S), metallic Co (Co), metallic Ni (Ni), GaAs (As).

4. Results

For purpose of this paper, we have adopted the mineral succession scheme of Litochleb (1984). Most samples were represented by massive, white to light gray quartz gangue usually free of macroscopic aggregates of ore minerals. Although no scheelite or K-feldspar was identified in our samples, we denote the massive quartz gangue as quartz-1. As quartz-2 are termed here quartz crystals that grew in open fractures or extension gashes or that precipitated on the walls of massive quartz-1 veins after their tectonic reactivation (Fig. 2a–b). The quartz-2 may be overgrown by calcite gangue with sulfides (arsenopyrite, pyrite; Fig. 2b–e). Chlorite is usually younger than calcite and fills spaces in the gangue (Fig. 2c). Muscovite is older than calcite and was found as co-genetic solid inclusions in quartz-2 (Fig. 3e; sample KB-3) or in various assemblages that overgrow the quartz-2 (e.g. muscovite-chlorite or arsenopyrite-muscovite-chlorite intergrowths; Figs 2c and 2g). Calcite may be present in more than one generation as indicated by the large range of its isotope composition. A brief description of the individual samples is given in the Appendix.

4.1. Chlorite chemistry and thermometry

Chlorite was studied in detail in two texturally distinct samples. In KB-10, the chlorite fills in large drusy cavi-

ties in the quartz gangue and is therefore younger than the quartz-1 host. Mineral paragenesis of the sample KB-15 is more complex and chlorite occurs as: i) rare isolated inclusions at the rims of the quartz-2 crystals (i.e., it is co-genetic with the youngest growth zone of quartz-2; Fig. 2e); ii) chlorite films along some grain boundaries between quartz-2 and calcite; iii) inclusions in the calcite gangue (i.e., co-genetic with calcite; Fig. 2f); iv) fracture fillings in the same calcite (i.e. younger than calcite), and v) as part of complex arsenopyrite-chlorite-muscovite intergrowths along vein contacts (Fig. 2c).

Despite this apparent complexity, no significant differences were found in chlorite chemistry and all the above-mentioned textural types in both samples can be considered to belong to a single chlorite generation (chlorite-1). However, in BSE images it is possible to see that the predominating chlorite-1 is locally replaced or overgrown by younger chlorite-2 (Fig. 2g).

All the studied chlorites (of both generations) correspond to the tri-trioctahedral group, based on the Wiewióra and Weiss (1990) classification. Representative chemical analyses and empirical crystallochemical formulae are given in Tab. 1. The proportion of vacancies (\square) in the octahedral site is less than 0.2. Minor compositional variations are attributed to a replacement of Si by divalent cations (R^{2+} , i.e. Fe, Mg, Mn) expressed as $(\text{Si}\square)_{-2}\text{R}^{2+}_2$ substitution. These variations reflect formation of late chlorite: e.g. in the sample KB-10 the Mg- and Si-rich chlorite-1 ($\text{Fe}/(\text{Fe} + \text{Mg})$: 0.359 ± 0.115 ; Si: 3.339 ± 0.152 apfu) is overgrown (replaced along grain boundaries?) by Fe-rich and Si-poor chlorite-2 ($\text{Fe}/(\text{Fe} + \text{Mg})$: 0.665 ± 0.03 ; Si: 2.879 ± 0.129 apfu). In the sample KB-15, some chlorite-1 grains are slightly richer in Si (3.304 ± 0.071 apfu) than the rest (3.229 ± 0.093 apfu); significant differences in contents of other elements or in the Fe/Mg ratio were not found, though (Tab. 1).

In order to constrain the chlorite formation temperatures, several chlorite thermometers were employed. Temperatures based on the given single calibration always vary only slightly (± 3 °C to ± 14 °C), however, the differences between individual thermometers are much greater (Tab. 1). The equations of Cathelineau and Nieva (1985) and Zhang and Fyfe (1995) yielded similar results (average: 268 ± 14 °C for KB-10 and 278 ± 9 °C for KB-15). These were *c.* 60 °C lower than the average temperatures based on the equations of Cathelineau (1988) or Jowett (1991) (332 ± 10 °C for KB-10 and 343 ± 13 °C for KB-15). The Fe-rich chlorite of sample KB-10 apparently formed at lower temperatures (257 ± 14 °C) than the Mg-rich chlorite of the same sample (277 ± 5 °C), based on Cathelineau and Nieva (1985) and Zhang and Fyfe (1995) calibrations.

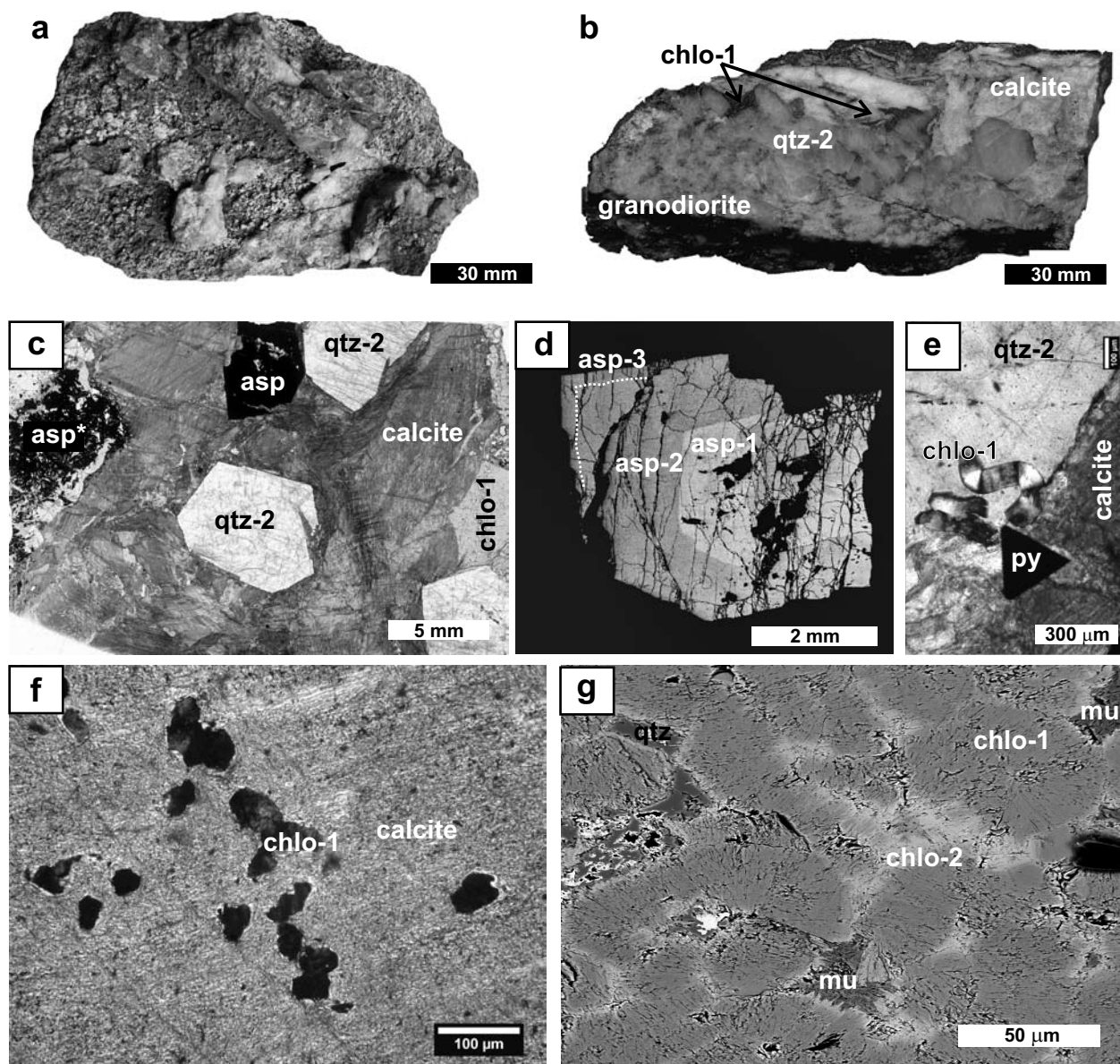


Fig. 2 Photographs of quartz-calcite gangue and of ore minerals from the Bělčice deposit. **a** – Fracture plane in granodiorite with crystals of quartz-2. **b** – Sample of quartz-calcite vein from the “Na Skřipici” mine. Quartz-2 (gray, qtz-2) is overgrown by calcite (white). Chlorite (dark, chlo-1) filled in the remaining space. **c** – Early calcite gangue (KB-15, scanned thin section) enclosing quartz-2 (qtz-2) and arsenopyrite (asp) crystals. Chlorite (chlo-1) fills in the remaining spaces. Arsenopyrite intergrowths with muscovite and chlorite are marked “asp*”. **d** – Back-scattered electron image of zoned arsenopyrite (asp) crystal from sample KB-15. The crystal core is Ni-, Co- and As- rich. **e** – Chlorite crystals (chlo-1) set in quartz-2 (qtz-2) matrix. Pyrite (py) is enclosed in calcite (plane polarized light). **f** – Grains of chlorite-1 (chlo-1) enclosed in calcite gangue (sample KB-15; plane polarized light). **g** – Back-scattered electron image of chlorite from sample KB-10. Medium-gray aggregates of chlorite-1 (chlo-1) are overgrown by chlorite-2 (chlo-2, whitish). Muscovite (mu) replaces chlorite and quartz-2 (qtz) is preserved only in relics.

4.2. Arsenopyrite chemistry

The arsenic content of arsenopyrite can be used as thermometer if independent sulfur fugacity estimation can be made (Kretschmar and Scott 1976; Sharp et al. 1985). Arsenopyrite was studied in sample KB-15

(Fig. 2c), where two textural associations were distinguished: i) about 10 mm large crystal embedded in calcite gangue and exhibiting zoning in BSE (Fig. 2d); and ii) small arsenopyrite crystals/grains distributed along the vein/granodiorite contact, homogeneous in BSE.

Tab. 1 Representative electron microprobe analyses (wt. % and recalculated on the basis of 14O) for chlorite from the Bělčice ore district and estimated temperatures of its formation

Sample	KB15	KB15	KB15	KB15 AVG	KB10	KB10	KB10	KB10 AVG	KB10	KB10	KB10 AVG
Analysis no.	10	13	11	n = 8	28	29	31	n = 5	30	34	n = 4
Type	chlo-1	chlo-1	chlo-1	chlo-1	chlo-1	chlo-1	chlo-1	chlo-1	chlo-2	chlo-2	chlo-2
SiO ₂	25.92	26.08	26.81	26.45	27.28	26.68	27.10	27.04	26.10	26.06	25.83
TiO ₂	0.08	0.06	0.00	0.04	0.00	0.04	0.06	0.03	0.03	0.00	0.01
Al ₂ O ₃	22.02	22.03	21.66	21.59	22.27	21.76	21.50	21.59	20.59	20.94	21.00
Cr ₂ O ₃	0.00	0.00	0.02	0.01	0.00	0.00	0.07	0.03	0.00	0.00	0.01
FeO _{tot}	21.39	20.52	20.12	20.35	19.51	19.59	18.38	19.03	32.69	30.87	31.56
MnO	0.24	0.44	0.11	0.29	0.31	0.31	0.19	0.20	0.09	0.00	0.04
MgO	17.78	17.88	17.49	17.75	18.41	18.32	20.18	19.10	7.59	10.15	8.94
CaO	0.05	0.12	0.03	0.04	0.02	0.06	0.03	0.03	0.06	0.10	0.06
Na ₂ O	0.00	0.00	0.03	0.01	0.04	0.01	0.05	0.02	0.00	0.00	0.00
K ₂ O	0.02	0.02	0.02	0.02	0.06	0.06	0.03	0.03	0.08	0.12	0.08
TOTAL	87.48	87.15	86.28	86.55	87.88	86.81	87.58	87.11	87.22	88.23	87.55
Si ^{IV}	2.677	2.695	2.780	2.745	2.767	2.747	2.747	2.764	2.866	2.801	2.810
Al ^{IV}	1.323	1.305	1.220	1.255	1.233	1.253	1.253	1.236	1.134	1.199	1.190
IV site	4.000	4.000	4.000	4.000	4.000	4.000	4.000	4.000	4.000	4.000	4.000
Al ^{VI}	1.358	1.377	1.428	1.385	1.428	1.389	1.317	1.365	1.531	1.453	1.503
Ti ^{VI}	0.006	0.004	0.000	0.003	0.000	0.003	0.004	0.002	0.003	0.000	0.001
Cr ³⁺	0.000	0.000	0.002	0.001	0.000	0.000	0.006	0.002	0.000	0.000	0.001
Fe ²⁺	1.848	1.773	1.745	1.766	1.655	1.687	1.559	1.627	3.002	2.774	2.872
Mn ²⁺	0.021	0.038	0.010	0.026	0.026	0.027	0.017	0.017	0.008	0.000	0.004
Mg ²⁺	2.738	2.752	2.703	2.745	2.783	2.812	3.049	2.910	1.242	1.626	1.449
vacancy	0.030	0.055	0.122	0.075	0.107	0.082	0.049	0.076	0.214	0.147	0.171
VI site	6.000	6.000	6.000	6.000	6.000	6.000	6.000	6.000	6.000	6.000	6.000
Ca	0.005	0.014	0.003	0.004	0.002	0.006	0.003	0.004	0.006	0.011	0.007
Na	0.000	0.000	0.007	0.001	0.008	0.003	0.009	0.004	0.000	0.000	0.000
K	0.003	0.002	0.002	0.002	0.007	0.008	0.003	0.004	0.011	0.016	0.011
TOTAL	10.000	10.000	10.000	10.000	10.000	10.000	10.000	10.000	10.000	10.000	10.000
Fe/(Fe+Mg)	0.403	0.392	0.392	0.391	0.373	0.375	0.338	0.359	0.707	0.631	0.665
T1	298	295	276	284 ± 9	279	283	283	280 ± 4	258	272	270 ± 8
T2	277	274	268	272 ± 3	269	271	274	272 ± 2	256	264	261 ± 4
T3	293	290	272	279 ± 10	276	280	284	278 ± 4	224	245	240 ± 11
T4	364	358	331	342 ± 14	335	341	341	336 ± 6	303	324	321 ± 13
T5	366	360	333	344 ± 14	336	343	341	337 ± 6	315	334	332 ± 12
T6	303	286	248	272 ± 19	252	267	285	269 ± 12	180.2	224	210 ± 21

Thermometers used: T1 = Cathelineau and Nieva (1985) (Al^{IV}); T2 = Cathelineau and Nieva (1985) (VI-vacancy); T3 = Zhang and Fyfe (1995) (Al^{IV}, Fe/Mg), T4 = Cathelineau (1988) (Al^{VI}); T5 = Jowett et al. (1991) (Al^{IV}, Fe/Mg); T6 = de Caridad et al. (1993) (VI-vacancy)

The former type of (zoned) arsenopyrite exhibits three compositionally different growth zones: a Ni, Co and As enriched core (asp-1; up to 0.95 wt. % of Ni and 0.65 wt. % of Co, with 35.18 to 35.66 at. % As), surrounded by a Ni, Co and As-poor intermediate zone (asp-2) and rim (asp-3) (< 0.20 wt. % of Ni or Co; and 32.711 to 31.872 at. % As). Arsenopyrite of the latter type (from the contact between granodiorite and vein) is chemically identical with that from the intermediate to rim zones (asp-2, asp-3).

Minimum and maximum temperatures of arsenopyrite formation were estimated from the intersection of arsenic isopleths (at. % As; Kretschmar and Scott 1976) with relevant sulfide univariant boundaries. These limits were

set at 455 ± 20 °C (arsenopyrite = pyrrhotite + loellingite) and 525 ± 15 °C (arsenopyrite + native arsenic = loellingite) for the core zone, at 350 ± 30 °C for the intermediate zone and at 350 ± 15 °C for the rim zone (arsenopyrite + native arsenic = loellingite).

4.3. Fluid inclusions

Three principal types of fluids were distinguished: aqueous-carbonic, carbonic and aqueous. Aqueous-carbonic with carbonic fluids were older than the aqueous fluids and can be found in quartz-1 only. Fluid inclusions, irrespective of the fluid type, are usually smaller than 20 µm. All the inclusions were measured only in quartz. Those

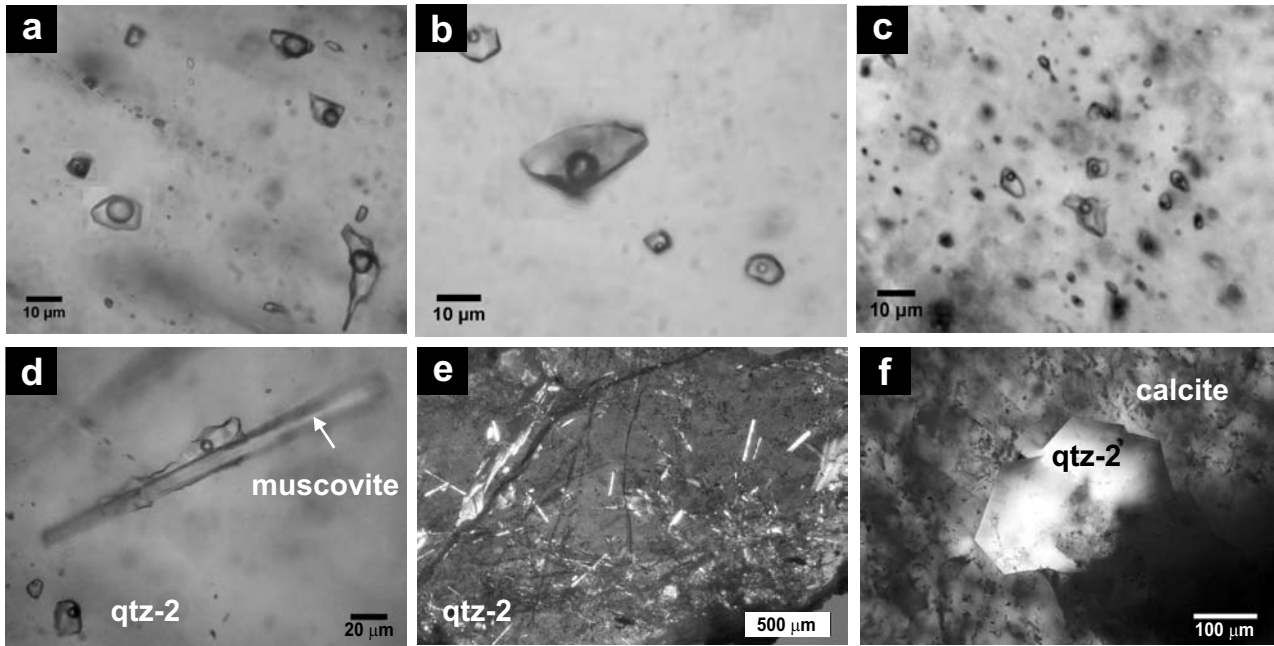


Fig. 3 Fluid inclusion photomicrographs (plane polarized light unless specified otherwise). **a** – Aqueous-carbonic inclusions (Lwc) in massive quartz-1 of sample KB-12. **b–c** – Aqueous inclusions (Lw) in massive quartz-2 of sample KB-15. **d** – Aqueous inclusion (Lw) that is attached to trapped muscovite (mu); sample KB-3. **e** – Quartz-2 (qtz-2) with numerous solid inclusions of muscovite (photo in crossed nicols; sample KB-3). **f** – Crystal of late quartz-2 (qtz-2) that is enclosed in calcite gangue (sample KB-18). Calcite is full of dark and too tiny fluid inclusions, while quartz contains rare and measurable aqueous inclusions (Lw).

in calcite were either too small, or were not transparent enough.

4.3.1. Liquid-rich aqueous-carbonic inclusions in quartz-1 (Lwc type)

Fluid inclusions of this type are two-phase liquid-rich at room temperature (Fig. 3a), consisting of homogeneous carbonic bubble enclosed in aqueous liquid. In relatively undeformed quartz gangue they also exhibit a homogeneous degree of fill (0.85 to 0.80; Tab. 3). In more deformed samples, the values of the degree of fill are more scattered. The Lwc inclusions are mostly oval in shape and represent the most frequent CO₂-bearing inclusion type.

The melting temperature of solid CO₂ (Tm-CO₂) ranges from –59.6 °C to –56.6 °C (Tab. 3), with a marked frequency maximum at around –58.8 °C (Fig. 4a). The temperature of partial homogenization of CO₂ (Th-CO₂) varies from +3.7 to +20.1 °C (to the liquid state), or from +10.0 to +18.5 °C (to the vapor state). The CO₂ phase most frequently homogenizes from +10 to +15 °C (to both states; Fig. 4b and Tab. 3), suggesting only minor CO₂-density variations for each homogenization mode.

No significant differences in Tm-CO₂ and Th-CO₂ were found between the individual samples. The Tm-CO₂ data indicating relatively pure CO₂ are, however, much less

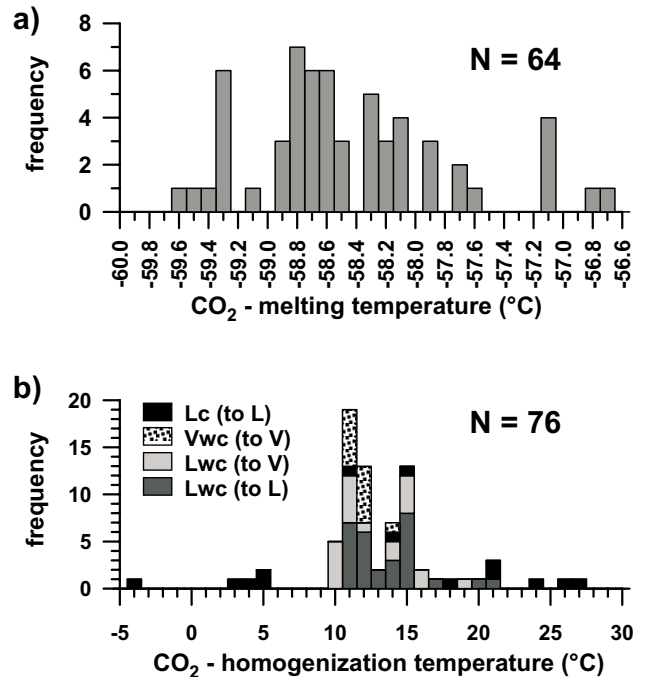


Fig. 4 Summary of the microthermometric characteristics of the carbonic phase in aqueous-carbonic inclusions (Lwc). **a** – Temperature of melting for solid CO₂, **b** – Temperature of partial homogenization for CO₂. The symbol “L+V = L” denotes homogenization to the liquid state, while “L+V = V” denotes final homogenization to the vapor.

Tab. 2 Representative electron microprobe analyses of arsenopyrite from the Bělčice ore district (wt. % and recalculated As at. %; sample KB-15)

Analysis no.	3	14	8	13	5	12	6	4	9	1	11	2	10	17	15	16
Type	asp-1	asp-1	asp-1	asp-1	asp-1	asp-1	asp-2	asp-2	asp-2	asp-2	asp-2	asp-2	asp-2	asp-2	asp-1	asp-1
Fe	32.76	32.63	33.00	32.74	32.94	33.25	33.48	34.29	35.02	34.17	34.95	34.80	34.91	35.07	34.94	34.96
Co	0.94	0.84	0.85	0.76	0.87	0.95	0.37	0.09	0.01	0.22	0.10	0.04	0.16	0.02	0.16	0.10
Ni	0.54	0.65	0.44	0.57	0.49	0.43	0.42	0.22	0.02	0.05	0.03	0.08	0.00	0.00	0.16	0.02
As (wt. %)	48.52	48.54	48.41	47.96	48.03	47.99	47.34	47.12	45.45	44.68	44.90	44.80	45.09	45.01	44.82	44.24
S	17.85	17.99	17.92	17.99	18.12	18.00	18.48	18.99	19.89	20.13	20.26	20.35	20.60	20.39	20.31	20.33
Total	100.62	100.65	100.62	100.00	100.46	100.62	100.09	100.71	100.38	99.25	100.25	100.06	100.76	100.49	100.40	99.65
As (at. %)	35.66	35.63	35.54	35.37	35.24	35.18	34.70	34.17	32.71	32.40	32.23	32.19	32.15	32.23	32.11	31.87

Tab. 3 Summary of microthermometric characteristics of aqueous-carbonic and carbonic inclusions (average $\pm 1\sigma$) from the Bělčice ore district

Type ¹	Sample	F	Tm-CO ₂ (°C)	Td-Cla (°C)	Th-CO ₂ (°C)	Th-tot (°C)	N ²		
Lwc	KB-2	0.85	-57.7 \pm 1.0	n.a.	14.1 \pm 0.4	L	311.8 \pm 8.2	L	9
	KB-2	0.90	-58.7 \pm 0.5	8.6 \pm 0.5	11.2 \pm 0.6	L	259.8 \pm 9.7	L	13
	KB-6	0.80	-58.2 \pm 0.2	n.a.	15.1 \pm 3.1	L	n.a.	-	3
	KB-2	0.85	-58.3 \pm 1.2	9.1 \pm 0.3	13.9 \pm 2.1	V	295.3 \pm 20.7	L	5
	KB-6	0.80	-58.2 \pm 1.1	9.1 \pm 0.5	11.9 \pm 2.5	V	298.1 \pm 15.1	L	21
Vwc	KB-2	0.15	-56.6 \pm 0.0	-	12.3 \pm 1.6	V	320.8 \pm 7.8	V	2
	KB-2	0.15	-58.7 \pm 0.4	-	11.0 \pm 0.2	V	259.1 \pm 4.2	V	11
Lc	KB-6	0.05	-58.8 \pm 0.2	-	6.7 \pm 5.4	L	-	-	4

Notes: ¹Fluid inclusion type: Lwc – liquid-rich aqueous-carbonic inclusions; Vwc – vapor-rich aqueous-carbonic inclusions; Lc – carbonic inclusions; ²N – number of measured inclusions. For explanation of other abbreviations see the relevant methodic chapter in the text.

frequent than those suggesting significant admixtures of other gases (CH₄ and/or N₂; corresponding to between 4–5 and 15–17 mol. % CH₄ in terms of simple binary CO₂-CH₄ mixture, based on Thiéry et al. 1994).

The clathrate dissociates at +7.5 to +10.1 °C (Td-Cla), at a temperature that is always lower than that of partial homogenization (Th-CO₂). Fluid salinity, estimated from Td-Cla and corrected for the admixture of CH₄, varies from 3 to 5.1 (sample KB-6) or from 4.4 to 6.8 wt. % eq. NaCl (sample KB-2).

Final homogenization of Lwc inclusions occurred at +249 °C to +326 °C to the liquid state (Fig. 5b and Tab. 3).

4.3.2. Vapor-rich aqueous-carbonic inclusions in quartz-1 (Vwc type)

Two-phase vapor-rich inclusions typically constitute no more than 5 % of all inclusions in the given sample. They are randomly distributed among Lwc inclusions and seem to be more frequent in samples affected by ductile deformation. The degree of fill (F) ranges from 0.1 to 0.3; the shape and size are similar to Lwc inclusions.

The Tm-CO₂ varies mostly from -58.1 °C to -59.3 °C, the Th-CO₂ from 10.5 to 11.2 °C (always to vapor) and the Th-tot from 265.4 to 253.5 °C (to vapor). Few inclu-

sions exhibited higher Tm-CO₂ (-56.6 °C) and Th-tot (315.2 to 326.4 °C, to vapor) values, but similar Th-CO₂ (11.2 to 13.4 °C, to vapor).

4.3.3. Carbonic inclusions in quartz-1 (Lc type)

Carbonic inclusions contain only homogeneous carbonic liquid phase. Due to likely presence of an invisible water film on inclusion walls, the degree of fill (F) was set to estimated 0.05 in fluid density calculations. The Lc inclusions are randomly distributed among Lwc inclusions and preferably hosted by ductile-deformed sample domains. The temperature of melting for solid CO₂ (Tm-CO₂) varies from -59.1 °C to -58.5 °C, and the temperature of partial homogenization of CO₂ (Th-CO₂) from -4.1 to +26.1 °C (to the liquid). Admixture of CH₄ in the carbonic phase is estimated at 6 to 15 mol. %.

4.3.4. Aqueous inclusions (Lw type) in quartz-1 and quartz-2

The aqueous (Lw) inclusions are two-phase liquid-rich at room temperature. They always exhibit a homogeneous degree of fill (0.90 to 0.95; Figs 3b–c). In quartz-1 most of them form trails and can therefore be classified as

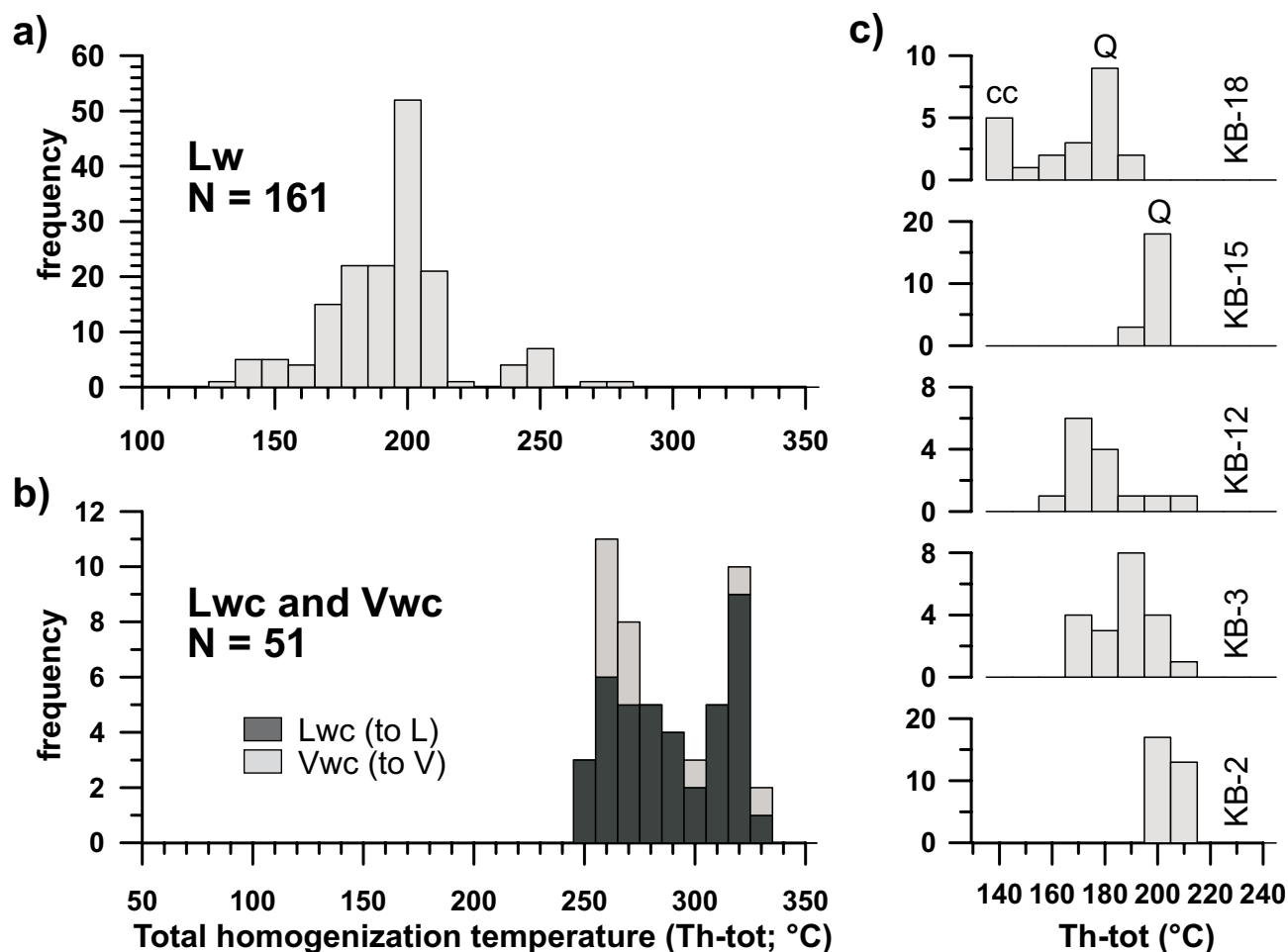


Fig. 5 Histograms of final homogenization temperatures (Th-tot) for individual fluid types and samples: **a** – summary histogram for aqueous inclusions (Lw); **b** – summary histogram for aqueous-carbonic inclusions (Lwc); **c** – aqueous inclusions in quartz – data for individual samples. Secondary inclusions in quartz that might be an equivalent of primary inclusions in calcite are labeled by “CC”. Inclusions in calcite were too small and dark to be measured. The symbol “L+V = L” denotes homogenization to the liquid state, while “L+V = V” denotes final homogenization to the vapor.

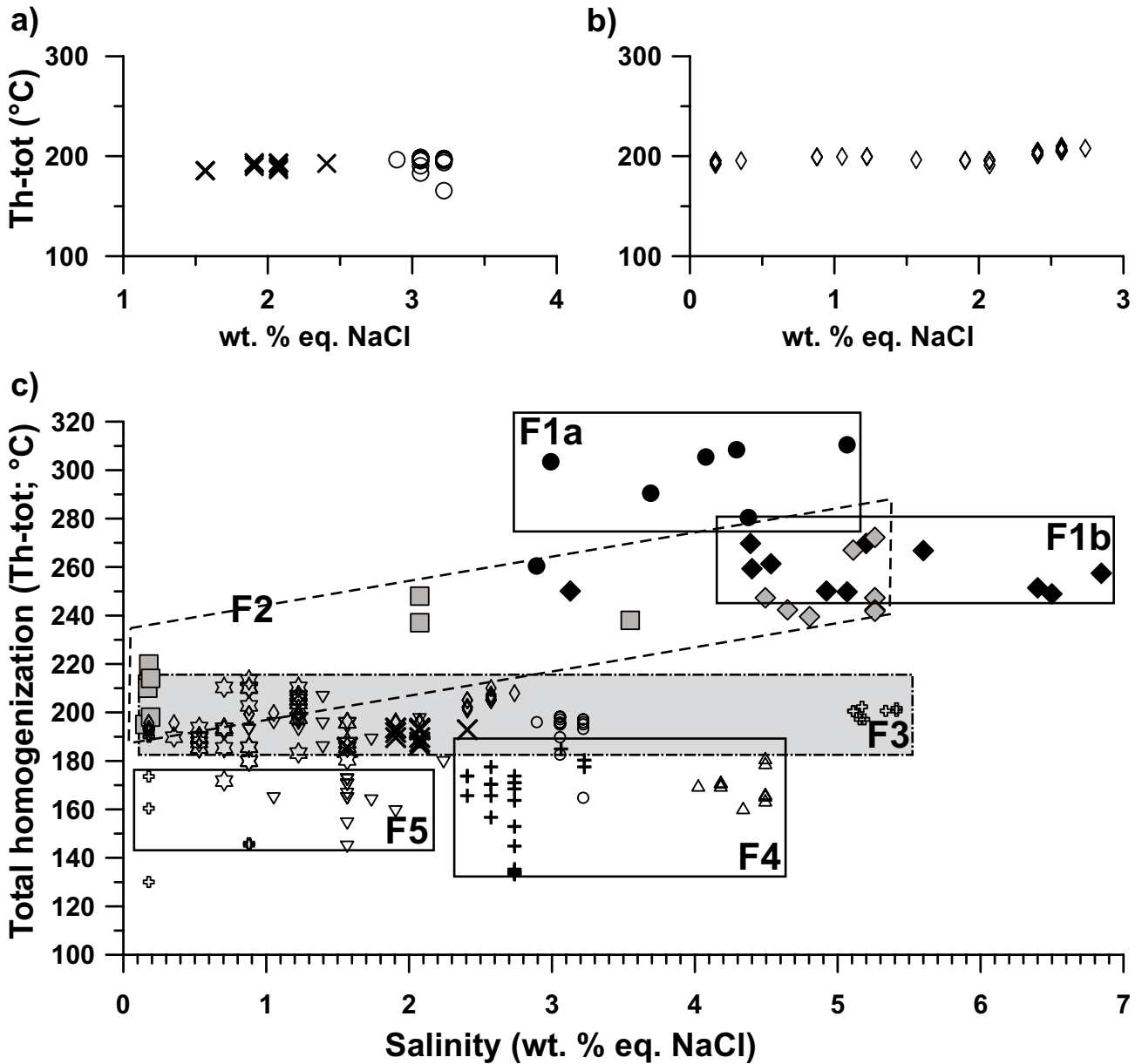
Tab. 4 Summary of microthermometric characteristics of aqueous inclusions from the Bělčice ore district

Mineral	Type ¹	Sample	Tm-ice (°C)	wt.% eq. NaCl	Th-tot (°C)		N ²
Qtz-1	S	KB-2	-1.6 to -0.1	2.7 to 0.2	210.0–191.2	L	30
	S	KB-6	-3.3 to -3.1	5.4 to 5.1	202.3–197.1	L	8
	S	KB-6	-1.2	2.1	190.8–187.6	L	3
Qtz-2	P	KB-15	-1.9 to -0.9	3.2 to 1.6	197.8–182.2	L	33
	P-PS	KB-3	-0.9 to -0.2	1.6 to 0.4	213.3–179.9	L	53
	?	KB-12	-3.2	5.3	272.2–247.3	L	5
	S	KB-12	-1.3 to -0.6	2.2 to 1.1	206.3–159.1	L	14
	PS?	KB-18	-1.9 to -1.4	3.2 to 2.4	184.9–156.7	L	16
	S	KB-18	-1.6	2.7	152.9–133.2	L	7

Notes: ¹Fluid inclusion type: P – primary, PS – pseudosecondary, S – secondary; ²N – number of measured inclusions. For explanation of other abbreviations see the text.

secondary. In quartz-2 Lw inclusions form, besides secondary trails, also three-dimensional clusters (samples KB-3, KB-15) or short intragranular trails not crossing grain boundaries (KB-3 only). Such inclusions can be

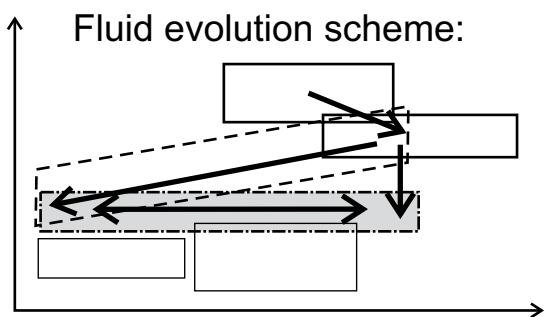
considered as primary or pseudosecondary. The primary nature of Lw inclusions in the sample KB-3 (quartz-2) is further indicated by the rare presence of these inclusions attached to muscovite crystals (Fig. 3d) and by



Samples and inclusion types:

- KB-6 (H₂O-CO₂)
- ◆ KB-2 (H₂O-CO₂)
- ◇ KB-12 (H₂O) – isolated inclusions
- KB-6 (H₂O) – isolated inclusions
- ◇ KB-2 (H₂O) – secondary incls., trails
- ☆ KB-3 (H₂O) – secondary incls., trails
- ⊕ KB-6 (H₂O) – secondary incls., trails
- ▽ KB-12 (H₂O) – secondary incls., clusters
- △ KB-12 (H₂O) – secondary incls., trails
- ⊗○ KB-15 (H₂O) – primary inclusions
- + KB-18 (H₂O) – primary & secondary incls.

d)



the frequent presence of muscovite inclusions in quartz grains (Fig. 3e).

The temperature of the first melting was difficult to determine accurately; however, melting was already in progress at $-35\text{ }^{\circ}\text{C}$. Therefore, for most Lw inclusions only the temperature of melting of the last ice crystal ($T_{\text{m-ice}}$: -3.9 to $-0.1\text{ }^{\circ}\text{C}$) and final homogenization temperature ($T_{\text{h-tot}}$) were measured ($T_{\text{h-tot}}$: $+130$ to $+272\text{ }^{\circ}\text{C}$, to liquid; Fig. 6c). Individual Lw inclusion assemblages usually exhibited only minor variations in the measured microthermometric parameters (see also Fig. 6c).

The salinity varies from 0.2 to 5.4 wt. % eq. NaCl. For most samples, moderate salinity variations are coupled with minor variations in the final homogenization temperatures, suggesting isothermal mixing (e.g. Figs 6a–b). Primary to pseudosecondary Lw inclusions in the quartz-2 (sample KB-15) exhibit a core-to-rim increase in the salinity under more or less constant $T_{\text{h-tot}}$ (Fig. 6a).

Summary homogenization data ($T_{\text{h-tot}}$) exhibit a pronounced frequency maximum at around $+200\text{ }^{\circ}\text{C}$ (Fig. 5a). In contrast, homogenization temperatures lower than $\sim 150\text{ }^{\circ}\text{C}$ (measured on secondary inclusions only) are scarce and most probably correspond to fluids from which late calcite precipitated.

4.4. Stable isotopes in quartz and calcite

The oxygen isotope composition of the analyzed quartz-1 gangue varies from 12.1 to 13.6 ‰ SMOW (Tab. 5). Assuming that the quartz-1 formation temperatures corresponded to the highest homogenization temperatures of the Lwc inclusions ($\sim 330\text{ }^{\circ}\text{C}$) or even higher (up to $450\text{ }^{\circ}\text{C}$; arsenopyrite thermometer), the oxygen isotope composition of the hypothetical parental fluid would fall between $+8.5$ and $+11.0\text{ }^{\circ}\text{‰ SMOW}$.

Calcite of sample KB-15 is depleted in ^{13}C and in ^{18}O compared to late calcite (KB-18; Fig. 7 and Tab. 5). Taking into account the independently-derived calcite formation temperatures of $\sim 275\text{ }^{\circ}\text{C}$ for KB-15 (chlorite thermometry) and a range from $133\text{ }^{\circ}\text{C}$ (homogenization

⇐

Fig. 6 Relationships between the fluid salinity and final homogenization temperature ($T_{\text{h-tot}}$). **a** – Primary aqueous inclusions (Lw) in the crystal of quartz-2 (sample KB-15). The crosses represent inclusions in the crystal core, while the open circles inclusions from the crystal rim. **b** – Marked horizontal trend in data for four populations of secondary aqueous inclusion (Lw) trails in sample KB-2. The data are interpreted to reflect isothermal mixing in late fluids. **c** – Summary plot for all samples with discrimination of individual samples, inclusion generations and major fluid types (labeled F1 through F5). The sample and inclusion legend relates only to this figure. **d** – Schematic representation of distinguished fluid stages and fluid mixing trends (thick lines with arrows).

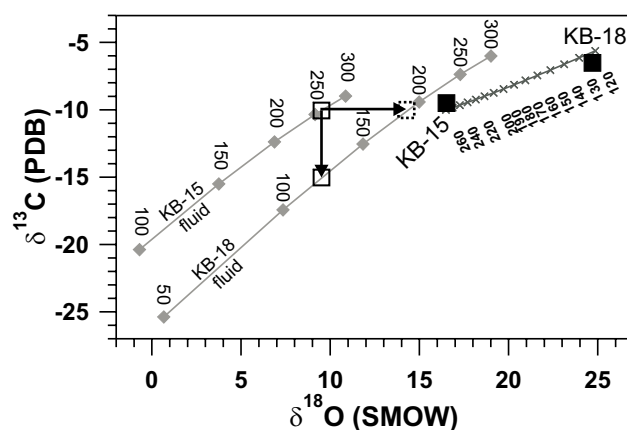


Fig. 7 Stable isotope data (black squares) for calcite of the ore stage (sample KB-15) and calcite of the late stage (sample KB-18). The thin line connecting the two samples delimits the theoretical composition of calcite in equilibrium with fluid ($\delta^{18}\text{O}_{\text{fluid}} = 10.3\text{ }^{\circ}\text{‰ SMOW}$ and $\delta^{13}\text{C}_{\text{fluid}} = -10.5\text{ }^{\circ}\text{‰ PDB}$) at temperatures indicated along the line (diagonal crosses, 260 to 120 $^{\circ}\text{C}$). The gray lines and diamonds delimit the hypothetical composition of a fluid that could have precipitated calcite with composition identical to samples KB-15 and KB-18. The lines are labeled by hypothetical temperatures of calcite precipitation. Solid thick arrows mark two alternative boundary trends in the composition of parental hydrothermal fluid (open boxes) during ore stage to late stage evolution. For more details see the discussion.

Tab. 5 Isotope composition of quartz and calcite gangue from the Bělčice ore district

Sample	Type	$\delta^{18}\text{O}_{\text{min}}$ (SMOW)	$\delta^{13}\text{C}_{\text{min}}$ (PDB)
KB-2	quartz-1	12.4	
KB-5	quartz-1	13.6	
KB-6	quartz-1	12.1	
KB-15	early calcite	16.5	-9.5
KB-18	late calcite	24.7	-6.5

temperatures of the latest fluids) to $185\text{ }^{\circ}\text{C}$ (homogenization temperatures of primary inclusions in quartz-2 that preceded the late calcite formation) for KB-18, then the oxygen isotope composition of the hypothetical parental fluid can be estimated at $+10$ to $+14\text{ }^{\circ}\text{‰ SMOW}$.

5. Discussion

5.1. P–T conditions of vein formation

The pressure and temperature evolution of gold-bearing quartz veins in the Bělčice ore district is summarized in Fig. 8. The homogenization temperatures of early Lwc inclusions in the sample KB-2 range from 315 to $326\text{ }^{\circ}\text{C}$. These temperatures represent the minimum formation temperatures of quartz-1. Similar and slightly higher temperatures (320 – $380\text{ }^{\circ}\text{C}$) were estimated for arsenopyrite-2 and arsenopyrite-3 based on Kretschmar

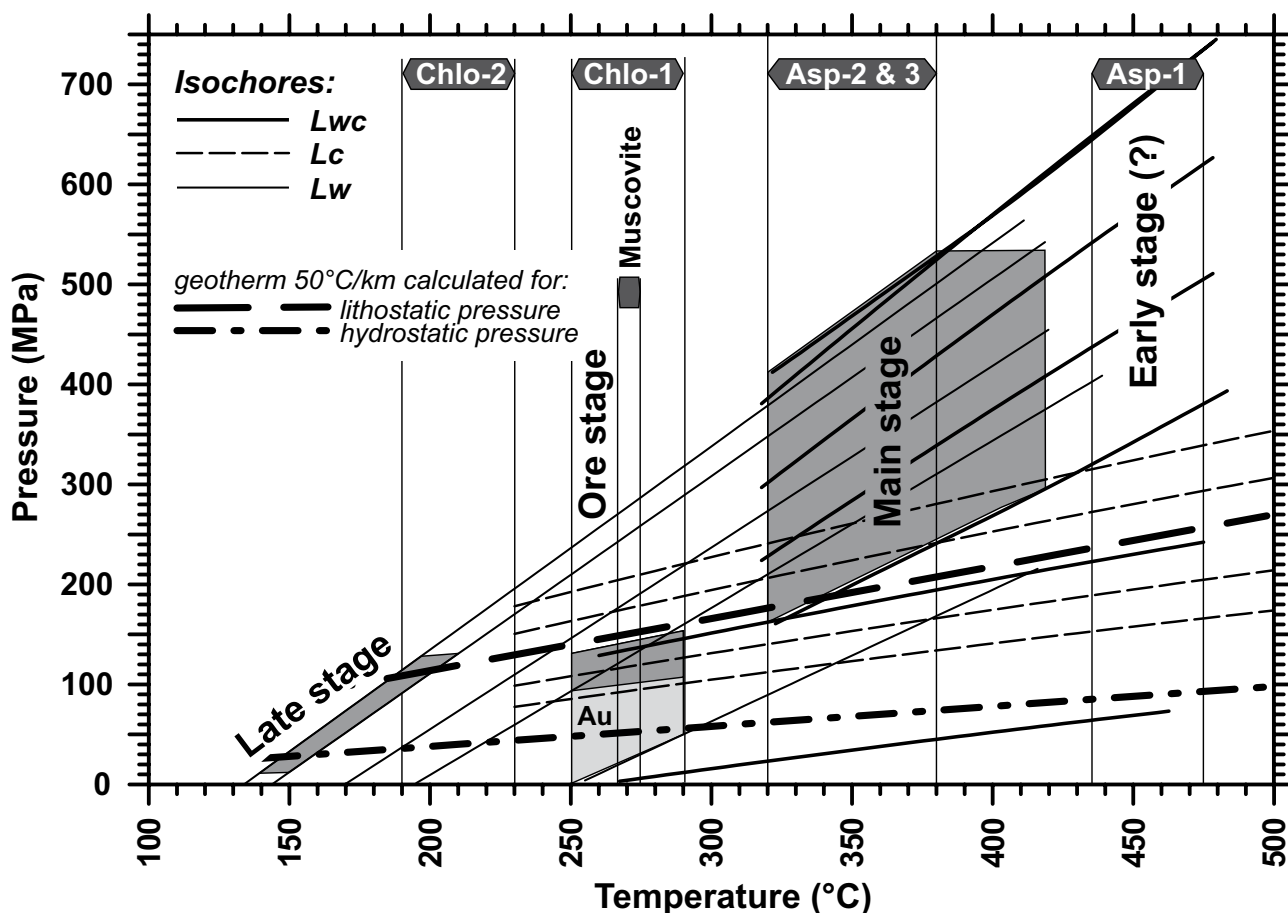


Fig. 8 Estimated P-T conditions of formation for the indicated mineralization stages, based on the mineral thermometry and representative fluid isochores. The probable temperatures of mineral formation, as calculated from the mineral chemistry, are indicated by dark hexagonal boxes along the upper horizontal axis (Chlo = chlorite, Asp = arsenopyrite). The box labeled “Au” denotes the probable conditions of gold precipitation.

and Scott (1976) thermometry. The most likely interval of quartz-1 precipitation is therefore 350 to 400 °C. Slightly higher temperatures are, however, still possible for early quartz-1, K-feldspar, scheelite, arsenopyrite-1 and tourmaline. For example, temperatures of about ~450 to 515 °C were estimated for a relic of arsenopyrite-1 enclosed in arsenopyrite-2. Temperatures up to ~500 °C are also estimated for quartz-1 and wolframite from the neighboring Kasejovice gold district, based on oxygen isotope thermometry (unpublished data of J. Zachariáš).

The lower and upper pressure limits of quartz-1 formation (~400 MPa and ~200 MPa, respectively) can be inferred from the range of Lwc and Lc isochores (Fig. 8). The value of ~400 MPa is equivalent to a depth of 14–15 km under a lithostatic pressure load. Finally, the difference between the maximum and minimum pressures (isochores) in the main and ore stages corresponds to the theoretical difference between fully lithostatic and fully hydrostatic conditions. This suggests significant pressure variations during quartz gangue evolution.

Based on fluid inclusion petrography, we suggest that Lc and Vwc inclusions might have originated from Lwc inclusions by partial leakage during subtle deformation of quartz-1 veins. The Lc and Vwc inclusions with the lowest fluid densities therefore probably reflect pressure load during deformation of the quartz-1 host (~100 to ~150 MPa). A similar response of fluid inclusions to tectonic decompression was demonstrated experimentally (Vityk and Bodnar 1998).

The quartz-2 is mostly younger than the deformation of quartz-1. Therefore we consider the same pressure range (~100 to ~150 MPa) as upper limit for formation of quartz-2. More accurate P-T conditions can be further obtained by intersection of the Lw (170 °C and 195 °C) and Lc isochores with temperatures based on independent mineral thermometers (250–290 °C; chlorite-1, muscovite; Fig. 8). With respect to mineral succession scheme of Litochleb (1984), the P-T conditions inferred for quartz-2 should also represent those of gold deposition.

Application of chlorite thermometry in general is hampered by the influence of the host rock environment on fluid–chlorite hydrothermal equilibrium and by analytical limitations in precise measurement of the Fe^{3+} and H_2O contents in chlorites (e.g., de Caritat et al. 1993). Therefore, none of existing chlorite thermometers ensures accurate estimation of the chlorite formation temperatures. In our case, the equations of Cathelineau and Nieva (1985) and Zhang and Fyfe (1995) yielded temperatures in the range of 258 to 288 °C, while those of Cathelineau (1988) or Jowett (1991) resulted in higher temperatures (342–380 °C). Therefore it can be safely assumed that most chlorites-1 were formed at temperatures higher than *c.* 250 °C.

In order to check the estimated temperatures, we further employed regression between the chlorite formation temperature and the occupancy of the octahedral site, as suggested by de Caritat et al. (1993) in their figure 8. Temperatures derived in this way (272 ± 17 °C for sample KB-15 and 269 ± 12 °C for the Mg-rich chlorite-1 of sample KB-10), are almost identical with those based on the equations of Cathelineau and Nieva (1985) and Zhang and Fyfe (1995). The temperature estimated for the Fe-rich chlorite-2 (210 ± 21 °C; sample KB-10) is, however, about 60 °C lower than that obtained using the Cathelineau and Nieva (1985) and Zhang and Fyfe (1995) thermometers. With respect to the late formation of chlorite-1 in the mineral paragenesis and to the measured homogenization temperatures of Lw inclusions (up to 270 °C), formation of most chlorites-1 at 290–250 °C is very likely. Lower temperatures (190–230 °C) are suggested only for the Fe-rich chlorite-2 of sample KB-10. This chlorite is visibly younger than the higher temperature one.

During the late stage, late calcite accompanied by rare sulfides crystallized from an aqueous fluid, the inclusion homogenization temperatures of which ranged from ~130 to ~150 °C.

5.2. Isothermal mixing of fluids

Aqueous fluid inclusions (Lw) in individual samples exhibit marked linear (subhorizontal) trends in the salinity – final homogenization temperature (Th-tot) plots (e.g. Figs 6a–b). These trends are usually interpreted as mixing trends. Two fluid end members can be distinguished: i) the higher-salinity end member (~ 5–5.5 wt. % NaCl eq.) – a likely product of gradual CO_2 outgassing from aqueous carbonic fluids (Lwc); and ii) the low-salinity end member (~ 0 wt. % NaCl eq.).

The observed mixing trends are schematically illustrated in Fig. 6d. Isolated Lw inclusions (F2 fluid box in Fig. 6c) in samples KB-12 and KB-6 chronologically represent the first inclusion type where the mixing trend

was recognized. Later, isothermal mixing predominated between the chilled higher-salinity end member and the thermally unmodified low-salinity end member (F3 fluid box in Fig. 6c). Samples KB-2 and KB-3 represent prominent examples of isothermal mixing. During the late fluid evolution, mixing trends are poorly discernible and simple cooling seems to have predominated (Fig. 6c; boxes labeled F4 and F5).

Fluid inclusion trails often exhibit preferential three-dimensional orientation, the formation of which can be correlated with regional stress field (e.g. Pécher et al. 1985). The presence of similarly oriented fluid inclusion trails with markedly different salinities (but nearly constant homogenization temperatures; e.g. sample KB-2) allows us to suggest either minor variations in the regional stress field (if the fluid mixing process was very slow), or to the contrary, very effective and rapid fluid mixing (under rapidly changing stress field patterns). We prefer the later option, especially due to the observed evidence for rapid cooling of the higher-salinity end member to temperatures equivalent to those of the low-salinity end member. Finally, the later fact also allows us to speculate that the low-salinity end member could have been in thermal equilibrium with the host rocks.

5.3. Isotope composition of mineralizing fluids and the fluid mixing model

The estimated oxygen isotope composition of the mineralizing fluids gradually increases from the main stage ($\delta^{18}\text{O}_{\text{fluid}} = +8.5$ to $+11$ ‰ SMOW; based on quartz-1 data) to the late stage ($\delta^{18}\text{O}_{\text{fluid}} = +10$ to $+14$ ‰ SMOW; based on quartz-2 and calcite data). The whole-rock oxygen isotope composition of the Blatná granodiorite (major host-rock type) varies between 7.0 to 8.1 ‰ SMOW (unpublished data of M. Pudilová), that of Moldanubian gneisses (metamorphosed clastic sediments) is unknown, but probably higher than $+12$ ‰. The observed gradual increase in $\delta^{18}\text{O}_{\text{fluid}}$ can be explained by a gradual change from fluids isotopically equilibrated with granitoids to fluids that equilibrated with country-rock metasediments. While the metamorphic nature of the later fluid is evident, the former one could be of magmatic (*sensu lato*) or of metamorphic origin.

The isotope composition of the late-stage fluid can be discussed in even more detail. Relevant is that the isotope composition of both calcites can be derived from one common parental fluid (Fig. 7). Fixing the fluid isotope composition at $+10.3$ ‰ SMOW ($\delta^{18}\text{O}_{\text{fluid}}$) and at -7.3 ‰ PDB ($\delta^{13}\text{C}_{\text{fluid}}$) yields calcite precipitation temperatures corresponding to 282 and 131 °C for samples KB-15 and KB-18, respectively. The estimated precipitation temperatures correspond well to the measured fluid inclusion homogenization temperatures (275 and 133 °C, respectively).

If the theoretical composition of the parental fluid is calculated for each calcite sample separately, then two slightly different scenarios can be envisaged (Fig. 7). In first, under more or less constant oxygen isotope composition of the parental fluid, the younger calcite (KB-18) must have had originated from a fluid about 5 ‰ enriched in ^{12}C compared to the older calcite (KB-15) and at temperatures similar to the homogenization temperatures of Lw inclusions in this calcite (133 °C). The second assumes a formation temperature of the younger calcite (KB-18) similar to the homogenization temperature (i.e. minimum trapping temperatures) of primary inclusions in the quartz-2 (~ 180 to 200 °C). If true, the isotope composition of the dissolved inorganic carbon would remain constant ($\delta^{13}\text{C}_{\text{fluid}} = -10$ ‰ PDB) during precipitation of both KB-15 and KB-18 calcites, but that of oxygen would increase from c. +10 to +14 ‰ SMOW ($\delta^{18}\text{O}_{\text{fluid}}$). Both scenarios are equally possible; the former one (constant oxygen but variable carbon) suggests interaction of late fluids (KB-18) with calc-silicate rocks depleted in ^{13}C (e.g. Žák and Sztacho 1994), or with organic carbon component in the rocks or in the tectonic zones. The latter scenario (variable oxygen but constant carbon) indicates sealing of fluid migration paths in the granodiorite host and gradually increasing the amount of fluids isotopically equilibrated with Moldanubian metamorphic rocks. Simple cooling of fluids equilibrated with solid granodiorite or with granitic magma can be excluded, as this would result in an opposite trend (decreasing values of $\delta^{18}\text{O}_{\text{fluid}}$).

6. Conclusions

The quartz veins at the Bělčice ore district (Central Bohemian Plutonic Complex) were formed from aqueous-carbonic fluids with significant methane admixtures (up to 15 mol. % of CH_4) at temperatures of c. 350–400 °C and pressures 200–400 MPa. The ore stage occurred at lower temperatures (250 to 300 °C) and pressures (~100 MPa), largely from aqueous fluids. The fluid pressure during both the main and ore stages varied between fully lithostatic and fully hydrostatic conditions.

The isotope composition of the quartz and carbonate gangue indicates progressively increasing values of the oxygen isotope composition of the parental fluid ($\delta^{18}\text{O}_{\text{fluid}}$; from original ~ +9 to +10 ‰ reaching +10 to +14 ‰ SMOW). This suggests invasion of metamorphic fluids equilibrated with Moldanubian metasedimentary rocks into the environment dominated by Variscan granitoids (the Blatná granodiorite). This explanation seems to be supported by simultaneous depletion of late fluids (late calcite) in ^{13}C , compared to previous fluid batches (early calcite), a feature than can be explained by carbon iso-

tope exchange with Moldanubian calc-silicate rocks or with metamorphosed carbonaceous matter. Invasion of external metamorphic fluids is also well supported by omnipresent isothermal or quasi-isothermal mixing trends in aqueous fluids (Lw inclusions).

To conclude, both the estimated isotope composition of fluids and the mineral formation temperatures are compatible with a fluid system dominated by metamorphic fluids. Unambiguous distinction between truly magmatic fluids (i.e. those expelled during magma crystallization) and magmatic-metamorphic fluids (i.e. those equilibrated with granitoid rocks under subsolidus conditions) during the early stage of the Bělčice vein evolution (early stage and incipient phases of the main stage) is, however, impossible based on isotope data alone. On the contrary, the isotope data demonstrated the unambiguously metamorphic nature of both the ore and late fluids and allowed us to exclude any involvement of meteoritic fluids in the studied system.

Acknowledgements. This research was supported by the Grant Agency of the Czech Republic, project No. 205/06/0702, by a Grant from the Ministry of Education to the Faculty of Science Charles University MSM0021620855 and by the UNESCO-IGCP project No. 540 "Fluid inclusions in orogenic Au deposits". Finally, we would like to thank I. Jačková (Czech Geological Survey) for carrying out the oxygen and carbon isotope measurements, A. Langrová (Academy of Sciences, Czech Republic) for assistance with microprobe analyses and P. Dobeš with J. Litochleb for their critical comments.

References

- BAKER T (2002) Emplacement depth and carbon dioxide-rich fluid inclusions in intrusion-related gold deposits. *Econ Geol* 97: 1111–1117
- BAKKER RJ (1997) Clathrates: computer programs to calculate fluid inclusion V-X properties using clathrate melting temperatures. *Comput and Geosci* 23: 1–18
- BAKKER RJ (1999) Adaptation of the Bowers and Helgeson (1983) equation of state to the $\text{H}_2\text{O}-\text{CO}_2-\text{CH}_4-\text{N}_2-\text{NaCl}$ system. *Chem Geol* 154: 225–236
- BODNAR RJ (1993) Revised equation and table for determining the freezing point depression of $\text{H}_2\text{O}-\text{NaCl}$ solutions. *Geochim Cosmochim Acta* 57: 683–684
- BOIRON MC, BARAKAT A, CATHELIN M, BANKS DA, ĎURIŠOVÁ J, MORÁVEK P (2001): Geometry and P-V-T-X conditions of microfissural ore fluid migration: the Mokrsko gold deposit (Bohemia). *Chem Geol* 173: 207–225
- BURROWS DR, SPOONER ETC (1987) Generation of a magmatic $\text{H}_2\text{O}-\text{CO}_2$ fluid enriched in Mo, Au, and W within

- Archean sodic granodiorite stock, Mink Lake, northwestern Ontario. *Econ Geol* 82: 1931–1957
- CATHELINÉAU M (1988) Cation site occupancy in chlorites and illites as a function of temperature. *Clay Min* 23: 471–485
- CATHELINÉAU M, NIEVA D (1985) A chlorite solid solution geothermometer: the Los Azufres (Mexico) geothermal system. *Contrib Mineral Petrol* 91: 235–244
- CLAYTON RN, MAYEDA TK (1963) The use of pentafluoride in the extraction of oxygen from silicates and oxides for isotopic analysis. *Geochim Cosmochim Acta* 27: 43–52
- CLAYTON RN, O'NEIL JR, MAYEDA TK (1972) Oxygen isotope exchange between quartz and water. *J Geophys Res* 77: 3057–3067
- DE CARITAT P, HUTCHEON I, WALSHÉ JL (1993) Chlorite geothermometry – a review. *Clays and Clay Min* 41: 219–239
- DÖRR W, FIALA J, FRANKE W, HAACK U, PHILIPPE S, SCHASTOK J, SCHEUVENS D, VEJNAR Z, ZULAUFG G (1998) Cambrian vs. Variscan tectonothermal evolution within the Teplá-Barrandian: evidence from U–Pb zircon ages of syntectonic plutons (Bohemian Massif, Czech Republic). *Acta Univ Carol, Geol* 42: 229–230
- GOLDFARB RJ, GROVES DI, GARDOLL S (2001) Orogenic gold and geologic time: a global synthesis. *Ore Geol Rev* 18: 1–75
- GROVES DI, GOLDFARB RJ, GEBRE-MARIAM M, HAGEMANN SG, ROBERT F (1998) Orogenic gold deposits: a proposed classification in the context of their crustal distribution and relationship to other gold deposit types. *Ore Geol Rev* 13: 7–27
- GROVES DI, GOLDFARB RJ, ROBERT F, HART CJR (2003) Gold deposits in metamorphic belts: overview of current understanding, outstanding problems, future research, and exploration significance. *Econ Geol* 98: 1–29
- HOFMANN A, SLAVÍK F (1913) The Kasejovice gold-bearing district. *Rozpr Čes Akad Věd, Umění, Tř. II*, 22: 1–44 (in Czech)
- HOLUB FV, COCHÉRIE A, ROSSI P (1997) Radiometric dating of granitic rocks from the Central Bohemian Plutonic Complex (Czech Republic), constraints on the chronology of thermal and tectonic events along the Moldanubian–Barrandian boundary. *C R Acad Sci Paris, Sciences de la Terre et des planètes* 325: 19–26
- JANOÚŠEK V, GERDES A (2003) Timing the magmatic activity within the Central Bohemian Pluton, Czech Republic: conventional U–Pb ages for the Sázava and Tábora intrusions and their geotectonic significance. *J Czech Geol Soc* 48: 70–71
- JOWETT EC (1991) Fitting iron and magnesium into the hydrothermal chlorite geothermometer. *GAC/MAC/SEG Joint Annual Meeting, Toronto, May 27–29, 1991, Program with Abstracts*, pp A62
- KOUTEK J (1946) Geology of the Kasejovice district with respect to new underground exploration activities. *Sbor St geol Úst Čs Republ* 13: 127–187 (in Czech)
- KRETSCHMAR U, SCOTT SD (1976) Phase relations involving arsenopyrite in system Fe–As–S and their application. *Canad Mineral* 14: 364–386
- LANG JR, BAKER T (2001) Intrusion-related gold systems: the present level of understanding. *Mineral Depos* 36: 477–489
- LITOCHEB J (1984) Gold-bearing veins in Újezdec near Bělčice (south Bohemia). *Acta Musei Bohemiae, České Budějovice* 24: 73–80 (in Czech)
- MALEC J, NOVÁK F (1982) Mineralogical and geochemical study of heavy minerals for the project “Geochemical heavy minerals prospection in the southwestern part of the Bohemian Massif”. Unpublished report of the Institute of Raw Materials, Kutná Hora (in Czech)
- MCCREA JM (1950) On the isotope chemistry of carbonates and a paleotemperature scale. *J Chem Phys* 18: 849–857
- MORÁVEK P, JANATKA J, PERTOLDOVÁ J, STRAKA E, ĎURIŠOVÁ J, PUDILOVÁ M (1989) Mokrsko gold deposit – the largest gold deposit in the Bohemian Massif, Czechoslovakia. *Econ Geol Monograph* 6: 252–259
- OHMOTO H, RYE RO (1979) Isotopes of sulfur and carbon. In: Barnes HL (ed) *Geochemistry of Hydrothermal Ore Deposits*. John Wiley & Sons, New York, pp 509–561
- O'NEIL JR, CLAYTON RN, MAYEDA TK (1969) Oxygen isotope fractionation in divalent metal carbonates. *J Chem Phys* 51: 5547–5558
- PÉCHER A, LESPINASSE M, LEROY J (1985) Relations between fluid inclusion trails and regional stress field: a tool for fluid chronology – an example of an intragranitic uranium ore deposit (northwestern Massif Central, France). *Lithos* 18: 229–237
- SHARP ZD, ESSENE EJ, KELLY WC (1985) A re-examination of the arsenopyrite geothermometer: pressure considerations and applications to natural assemblages. *Canad Mineral* 23: 517–534
- SOBOTKA J (1966) Kasejovice–Bělčice gold-bearing district of and its minerals. *Lecture Notes, National Museum, Prague*, pp 1–23 (in Czech)
- THIÉRY R, VAN DEN KERKHOF AM, DUBESSY J (1994) vX properties of CH₄–CO₂ and CO₂–N₂ fluid inclusions: modeling for T < 31°C and P < 400 bars. *Eur J Mineral* 6: 753–771
- THOMPSON JFH, SILLITOE RH, BAKER T, LANG JR, MORTENSEN JK (1999) Intrusion related gold deposits associated with tungsten-tin provinces. *Min Depos* 34: 323–334
- VÁŇA T ET AL. (1988) Bohemian Massif – verification of gold resources, Kasejovice–Bělčice area: project final report. Unpublished manuscript, Geoindustria, Prague, pp 1–65 (in Czech)

- VLAŠÍMSKÝ P, PIŠA M (1985) Prognoses of W–Mo ores in the Bělčice ore district. Unpublished report, Czech Geological Survey, Prague, (in Czech)
- VITYK MO, BODNAR RJ (1998) Statistical microthermometry of synthetic fluid inclusions in quartz during decompression reequilibration. *Contrib Mineral Petrol* 132: 149–162
- WIEWIÓRA A, WEISS Z (1990) Crystallochemical classifications of phyllosilicates based on the unified system of projection of chemical compositions. *Clay Minerals* 25: 83–92
- ZACHARIÁŠ J, PUDILOVÁ M (2002) Fluid inclusion and stable isotope study of the Kasejovice gold district, central Bohemia. *Bull Czech Geol Surv* 77: 157–165
- ZACHARIÁŠ J, STEIN H (2001) Re–Os ages of Variscan hydrothermal gold mineralisations, Central Bohemian metallogenetic zone, Czech Republic. In: Piestrzyński et al. (eds) *Mineral Deposits at the Beginning of the 21st Century*, Swets & Zeitlinger Publishers Lisse, Amsterdam, pp 851–854
- ZACHARIÁŠ J., PUDILOVÁ M., ŽÁK K., MORÁVEK P., LITOUCHLEB J., VÁŇA T., PERTOLD Z. (1997): P–T conditions, fluid inclusions and O, C, S isotope characteristics of gold-bearing mineralizations within the Central Bohemian Metallogenetic Zone. *Acta Univ Carol, Geol* 41: 167–178
- ZACHARIÁŠ J, PERTOLD Z, PUDILOVÁ M, ŽÁK K, PERTOLDOVÁ J, STEIN H, MARKEY R (2001) Geology and genesis of Variscan porphyry-style gold mineralization, Petrůvkova hora deposit, Bohemian Massif, Czech Republic. *Min Depos* 36: 517–541
- ZHANG W, FYFE WS (1995) Chloritization of the hydrothermally altered bedrock at the Igarapé Bahia gold deposit, Carajás, Brazil. *Min Depos* 30: 30–38
- ZHANG YG, FRANTZ JD (1987) Determination of the homogenization temperatures and densities of supercritical fluids in the system NaCl–KCl–CaCl₂–H₂O using synthetic fluid inclusions. *Chem Geol* 64: 335–350
- ŽÁK K, SZTACHO P (1994) Marbles, calc-silicate rocks and skarns of the Moldanubian Unit (Bohemian Massif): carbon and oxygen isotope and fluid inclusion constraints on their formation conditions. In: Nishiyama T, Fisher GW (eds) *Proceedings 29th International Geological Congress, Kyoto, Part A, Metamorphic Reactions: Kinetics and Mass Transfer*. VSP International Science Publishers, Zeist, pp 39–49

Appendix (list of samples)

The samples are from dumps of the Barbora adit in Újezdec near Bělčice unless stated otherwise.

KB-2: granodiorite with a fragment of a more than 5 cm thick massive quartz vein (quartz-1) and another thick quartz vein *c.* 1 cm across (oriented approx. at 45° to the thicker vein) that seems to be crosscut by the thicker vein. Fluid inclusions were studied only in the thinner vein. In addition to the two quartz veins it is possible to identify several extensional fractures (more or less parallel with the thinner vein), incompletely filled with euhedral quartz and chlorite crystals.

KB-3: a fracture plane in granodiorite incompletely covered with crystals of quartz (quartz-2) and albite. Individual quartz-1 crystals are up to ~5 cm across and their *c*-axis is mostly parallel with the fracture plane (Fig. 2a). On a microscale numerous flakes of coarse-grained muscovite were found enclosed in the quartz-1 grains (i.e. muscovite had to have been cogenetic with this quartz; Fig. 3e). Fluid inclusions were studied in the largest quartz crystal.

KB-5: approximately 1 cm thick vein of massive milky quartz-1 with one 5 mm long grain of molybdenite.

KB-6: about 1 cm thick quartz vein (massive milky quartz-1) rimmed by fragments of fresh granodiorite.

KB-10: massive milky quartz-1 vein fragment. The gangue gradually evolves from coarse-grained massive into vuggy (drusy) gangue. The vugs are empty or filled with dark-green chlorite.

KB-12: fragment of massive milky coarse-grained quartz-1 vein.

KB-15: “Na Skřipici” mine, dumps. Some 2 to 3 cm thick hydrothermal vein consisting of massive quartz-2 and calcite gangue with sparse euhedral crystals of quartz-2 (Figs 2c–e). Rare vugs in the gangue are filled with coarse-grained, dark green chlorite. The contact between the granodiorite and the vein is locally coated with arsenopyrite crystals up to 5 mm in size.

KB-18: “Na Skřipici” mine, dumps. Breccia of hydrothermally altered granodiorite with irregular quartz-2 stringer (veinlets up to 5 mm thick) and fracture fillings of younger calcite. The sample evidently comes from a tectonic zone. Alteration is dominated by chlorite and white mica assemblage.